PHYSICAL REVIEW A VOLUME 31, NUMBER 5 MAY 1985

Pattern selection in a boundary-layer model of dendritic growth in the presence of impurities

Alain Karma and B. Gabriel Kotliar
Institute for Theoretical Physics, University of California, Santa Barbara, Santa Barbara, California 93106

(Received 5 December 1984)

We have analyzed, in the context of a boundary-layer model, the problem of pattern selection in dendritic growth in a situation where impurities are present in the undercooled liquid. We find that the tip-velocity selection criterion that has been proposed recently for the geometrical model and the boundary-layer model of a pure substance can be extended, in a nontrivial way, to this more complex situation where two coupled diffusion fields (temperature and solute) determine the interface dynamics. Our model predicts a sharp enhancement of tip velocity in good qualitative agreement with experiment. This agreement is consistent with the conjecture that a solvability condition can be used to determine the operating point of the dendrite in the full nonlocal problem.

I. INTRODUCTION

The search for an understanding of the mechanisms which govern the formation of geometrical patterns in nonequilibrium dissipative systems has been a continuing subject of interest in physics and biology. Well-known examples of patterns found in physical systems include the convection cells formed in Rayleigh-Bénard convection, the vortices formed in Taylor-Couette flow, and the dendritic, tree-like structures formed during the solidification of an undercooled liquid.

In the study of dendritic solidification a large part of the theoretical work has concentrated on predicting the properties of the needle-shaped dendritic tips.[1] These include the tip velocity and tip curvature, and the initial side-branch spacing. In order to avoid the mathematical and numerical difficulties encountered in the study of the full free-boundary problem of solidification, several authors have recently introduced local string models of interface dynamics. These include the geometrical model where the interface normal velocity is determined by the local curvature,[2,3] and the boundary-layer model (BLM) where part of the memory effects contained in the full problem are retained by allowing heat to diffuse along the interface.[4]

Both models have shown to be extremely useful in understanding the tip-velocity selection mechanism. In particular, it was shown that at nonzero surface tension only a discrete set of needle-crystal solutions to the steady-state equations can be found, and that the dynamically selected tip corresponds to the member of this discrete set with the maximum velocity.[5,6] The other members of the discrete set are all unstable and their number could possibly be infinite at small tip velocities.

A related problem in dendritic solidification, which has recently attracted both theoretical[7–9] and experimental[10] interest, is to understand the effect on the growth and morphology of the dendritic tip of adding a small amount of impurities to the undercooled melt.

This situation is very important technologically since it pertains to the solidification properties of dilute binary alloys. From a theoretical point of view it would be very interesting at this point to elucidate what mechanism determines the tip velocity when impurities are present in the melt. In particular, we would like to find out if the selection criterion that was developed in the context of the geometrical model and the BLM of a pure substance, applies in this more complex situation where both heat and solute diffusion fields are coupled at the interface. If the criterion applies, it would also be essential to know if it can be used to predict the enhancement in tip velocity at small impurity concentration which is seen experimentally.[10] Our motivation in examining this enhancement in tip velocity is that it has been understood previously in terms of a stability argument, which was used to perform quantitative calculations of dendritic growth rates and tip radii.[7–9] However, these calculations were all based on the assumption that the shape-preserving solutions of the steady-state equations consist of a continuous family of needle crystals. Since this assumption has been shown recently to be incorrect, at least for local models, it is very important to know at this point if a solvability condition, assuming it generalizes to the impurity problem, can predict this velocity enhancement. The main purpose of this paper is to answer these questions of selection and impurity effects, in the context of a string model (BLM) where both heat and solute are allowed to diffuse along the interface.

Our results show that, indeed, the selection criteria can be extended in the case where impurities are present. This is revealed, mathematically, by the existence of a one-parameter family of trajectories which flow into the two physical fixed points ($\theta=\pm\pi/2$) of the steady-state equations of our model.

This feature of the fixed points allows us to construct explicitly needle-crystal solutions to the steady-state equations and identify uniquely the dynamically selected tip velocity. In this way we are able, within the context of our model, to treat exactly the effects of impurities on dendritic growth. We find that at small solute concentration the tip velocity is enhanced initially and then decreases as the concentration is increased further. This is in complete qualitative agreement with what is seen experimentally, and is consistent with the speculation that a similar "needle-crystal" selection criterion holds in the full free-boundary problem.

This paper is divided as follows. In Sec. II we review the basic physics of dendritic growth in undercooled dilute solutions and derive the equations of motion for our model. In Sec. III we study the steady-state equations of the model and show how to construct needle-crystal solutions. In Sec. IV we discuss the results of our numerical simulations and finally in Sec. V we discuss the velocity enhancement at small impurity concentration.

II. DERIVATION OF THE MODEL

Consider a physical situation where a seed of solid is introduced in an undercooled binary liquid mixture where the concentration of solute is small. As the solid seed starts to grow a buildup of latent heat and solute appears at the interface. The latter is a result of the discontinuity in solute concentration at the interface, the solute concentration in the liquid being much greater than in the solid. In order for the seed to continue to grow the excess heat and solute need to diffuse away from the interface. Their rates of diffusion then control the rate of solidification of the interface. To be more specific consider a binary mixture with a phase diagram shown in Fig. 1. For simplicity we assume zero solubility of impurities in the solid, we neglect entirely the diffusion of heat in the solid, and we restrict our study to two dimensions. In the context of a string model we are primarily interested here in the qualitative features of the impurity problem and from this perspective we believe that these simplifications are not essential. In what follows we will use the following notation: T_M is the melting temperature for a pure substance, T_∞ and C_∞ are the temperature and solute concentration far from the interface, T_b and C_b are the temperature and solute concentration at the interface, L is the latent heat of fusion, C_p is the specific heat per unit volume in the liquid, β is the slope of the liquidus, D_1 and D_2 are, respectively, the diffusivity of heat and solute in the liquid, and Δ_e is the effective undercooling for a solute concentration C_∞, $\Delta_e=(T_M-T_\infty)/(L/C_p)-\beta C_\infty$. The temperature and solute concentration are written, respectively, as $T(\mathbf{x},t)$ and $C(\mathbf{x},t)$ where $\mathbf{x}$ is the two-dimensional position vector. It is also convenient to define a system of curvilinear coordinate $\theta(S)$, where $\theta(S)$ is the angle between the z axis and the local normal $\hat{n}(S)$ to the interface and S measures the arclength along the interface. These conventions are summarized in Fig. 2.

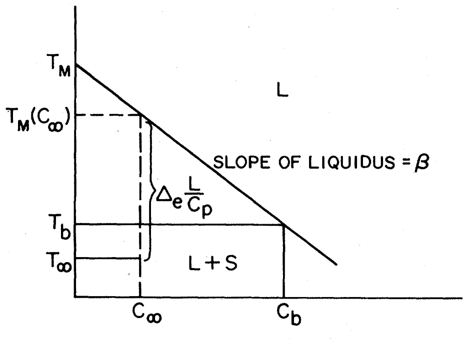

FIG. 1. Schematic phase diagram for a two-component system.

For convenience we also define the spatial diffusion fields

$$\tilde{u}_1(\mathbf{x},t)=\frac{T(\mathbf{x},t)-T_\infty}{L/C_p}\ , \tag{2.1}$$

$$\tilde{u}_2(\mathbf{x},t)=\frac{C(\mathbf{x},t)-C_\infty}{C_\infty}\ , \tag{2.2}$$

and their corresponding surface fields which are just the spatial fields evaluated at the interface:

$$u_i(S,t)=\tilde{u}_i(\mathbf{x},t)\,|_S \quad (i=1,2)\ . \tag{2.3}$$

The motion of the interface is then completely determined by the equations of motion for the spatial fields and their boundary conditions at the interface. The spatial fields obey the diffusion equation

$$\partial_t\tilde{u}_i=D_i\nabla^2\tilde{u}_i \quad (i=1,2)\ . \tag{2.4}$$

The first two boundary conditions are simply a statement of heat and solute conservation at the interface:

$$V_n=-D_1\hat{n}\cdot\nabla\tilde{u}_1\,|_{\text{interface}}\ , \tag{2.5}$$

$$V_n=-D_2\left.\frac{\hat{n}\cdot\nabla\tilde{u}_2}{(1+u_2)}\right|_{\text{interface}}\ . \tag{2.6}$$

Here the difference in form between the two continuity relations, Eqs. (2.5) and (2.6), comes from the fact that the heat rejected L is constant at any point on the interface but the solute rejected $C_b=(1+u_2)C_\infty$ can vary: The third boundary condition, the Gibbs-Thomson relation, is a statement of local thermodynamic equilibrium and couples the temperature with the solute concentration at the interface:

$$u_1+(\beta C_\infty)u_2=\Delta_e-\frac{T_MC_p}{L^2}\left[\gamma+\frac{\partial^2\gamma}{\partial\theta^2}\right]K\ .$$

Here $K\equiv\partial\theta/\partial S$ is the interface curvature and γ is the liquid-solid surface energy. In what follows we will assume a simple form of angular dependence with m-fold symmetry for γ:

$$\gamma=\gamma_0+\gamma_m\cos(m\theta)\ .$$

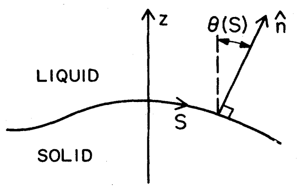

FIG. 2. Coordinate system.

It is then convenient to rewrite the Gibbs-Thomson relation in terms of a scaled capillary length d_0^1 and an effective anisotropy α such that

$$\frac{\alpha}{1+\alpha}=(m^2-1)\frac{\gamma_m}{\gamma_0}\ ,$$

$$d_0^1=\frac{T_M C_p \gamma_0}{L^2(1+\alpha)}\ ,$$

and

$$u_1+(\beta C_\infty)u_2=\Delta_e-d_0^1\{1+\alpha[1-\cos(m\theta)]\}K\ . \qquad (2.7)$$

In our numerical simulations, which will be described in Sec. IV, we used a fourfold anisotropy ($m=4$), and $\alpha=0.1$. This choice corresponds to a strength of anisotropy which is less than one percent ($\gamma_m/\gamma_0=1/165$), and corresponds roughly to the values of surface-tension anisotropy which have been measured for succinonitrile. For the geometrical model, it has been shown that the anisotropy strength has to be above a nonzero critical value for a tip steady state to be reached dynamically. In this paper we have not attempted to calculate this critical value for our model. However, the anisotropy strength $\alpha=0.1$ that we used in all our numerical simulations was always sufficient for a steady-state tip to be reached dynamically.

The free boundary problem defined by Eqs. (2.4)–(2.7) is very difficult to study both analytically and numerically. In particular, one has to solve the diffusion Eq. (2.4) everywhere in space in order to determine V_n via the continuity relations Eqs. (2.5) and (2.6). Another route is to project the problem onto the interface by Green's-function method.[11] This reduces the spatial dimensionality of the problem by 1 but the resulting integro-differential equation one obtains is nonlocal in space and time, and very hard to treat numerically. In order to avoid these difficulties, but hopefully still retain the essential physics of the problem, we make a boundary-layer approximation for the thermal and solute fields. A detailed discussion of the boundary-layer technique as it was first applied to the solidification of a pure substance can be found in Ref. 4. For completeness we will summarize here the essence of the approximation. Since the boundary-layer approximation applies to the thermal and solute fields equally well, we will keep the derivation of the equations of motion as general as possible by referring to the thermal and solute field by the index $i=1,2$, respectively.

The essence of the boundary-layer approximation is that instead of solving for the thermal and solute diffusion fields everywhere in space, we can characterize these fields by their effective thickness of warm fluid and excess solute ahead of the interface. Consider a typical profile of temperature or solute concentration at a given instant in time, along a direction η parallel to the local normal at S. This situation is described schematically in Fig. 3.

A good measure of the local thickness of excess solute or heat content is shown in Fig. 3 and can be written

$$l_i(S,t)=-\frac{u_i(S,t)}{\hat{n}\cdot\nabla\tilde{u}_i\,|_{\text{interface}}}\ . \qquad (2.8)$$

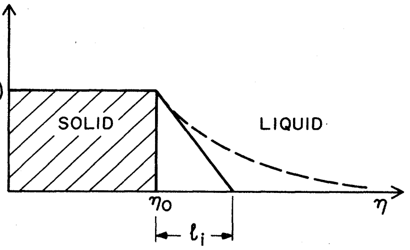

FIG. 3. Schematic temperature or concentration profile.

The two continuity relation equations (2.5) and (2.6) can be used to express V_n in terms of l_i:

$$V_n=\frac{D_1u_1}{l_1}\ , \qquad (2.9a)$$

$$V_n=\frac{D_2u_2}{l_2(1+u_2)}\ . \qquad (2.9b)$$

Now to completely specify the motion of the interface we need to specify some dynamics for l_i. As such it is not apparent how to write down an equation of motion for l_i and we eliminate l_i in terms of a new field H_i which corresponds to the excess heat or impurity content per unit length ahead of the interface:

$$H_i(S,t)\equiv\int_{\eta_0}^{\infty}\tilde{u}_i(\eta,t)d\eta\simeq u_i(S,t)l_i(S,t)\quad (i=1,2)\ . \qquad (2.10)$$

We can then derive an equation of motion for H_i by considering the time rate of change, along the normal growth direction ($d/dt\,|_n$), of the quantity $H_i\,\Delta S$. This quantity can change in two ways. First, heat or solute can be added to the boundary layer in a direction parallel to the local normal $\hat{n}(S)$. Second, heat or solute can diffuse along the interface. In a situation where the deformation of the interface varies slowly on the scale of l_i ($Kl_i\ll 1$), the contribution from these two processes can be treated separately. This situation will occur at large driving force Δ_e in which case V_n is large and l_i is small. Following this procedure we obtain

$$\left.\frac{d[H_i\,\Delta S]}{dt}\right|_n=\Delta S\,V_n(1-u_i\delta_{1,i})+\Delta S\,D_i\partial_S(l_i\partial_S u_i),\quad i=1,2 \qquad (2.11)$$

$$\delta_{1,i}=\begin{cases}1, & i=1\\ 0, & i=2.\end{cases}$$

The first term on the right-hand side of Eq. (2.11) corresponds to the addition of heat or impurities to the boundary layer along the local normal $\hat{n}(S)$. In the case of the thermal field the extra factor of $-\Delta S\,u_1V_n$ corresponds to the amount of heat needed to warm up the cold fluid just solidified to the local melting temperature. For a plane this first term on the right-hand side of Eq. (2.11) can be derived exactly and the details are given in Appendix A. The second term on the right-hand side of Eq. (2.11) corresponds to the addition of heat or solute by lateral diffusion where ∂_S denotes the gradient along the interface. Finally, we have to specify the equations of motion for ΔS and K:

$$\left.\frac{d\Delta S}{dt}\right|_n = \Delta S\, V_n K\,, \tag{2.12}$$

$$\left.\frac{dK}{dt}\right|_n = -(\partial_S^2 + K^2)V_n\,. \tag{2.13}$$

The derivation of the model is now complete. In order to simplify the form of the equations of motion and in order to work with dimensionless quantities we perform the following manipulations. We eliminate ΔS in Eq. (2.11) using Eq. (2.12), and also eliminate l_i everywhere in terms of H_i using Eq. (2.10). We scale all lengths in terms of d_0^1 and all times in terms of the "microscopic thermal diffusion time" $(d_0^1)^2/D_1$. Finally, we define a new set of dimensionless variables and parameters:

$$s=\frac{S}{d_0^1},\quad \tau=\frac{tD_1}{(d_0^1)^2},\quad v_n=V_n\frac{d_0^1}{D_1}\,,$$

$$\kappa=Kd_0^1,\quad r=\frac{D_2}{D_1},\quad h_i=\frac{H_i}{d_0^1}\quad (i=1,2)\,.$$

After performing these substitutions we obtain the following set of equations which completely specify our string model:

$$\left.\frac{dh_1}{d\tau}\right|_n = v_n(1-u_1) - v_n\kappa h_1 + \partial_s\left[\frac{h_1}{u_1}\partial_s u_1\right], \tag{2.14}$$

$$\left.\frac{dh_2}{d\tau}\right|_n = v_n - v_n\kappa h_2 + r\partial_s\left[\frac{h_2}{u_2}\partial_s u_2\right], \tag{2.15}$$

$$v_n = \frac{u_1^2}{h_1} = r\frac{u_2^2}{h_2(1+u_2)}\,, \tag{2.16}$$

$$\begin{gathered} u_1 + (\beta C_\infty)u_2 = \Delta_e - \kappa(1+f)\,, \\ f = \alpha[1-\cos(m\theta)]\,. \end{gathered} \tag{2.17}$$

The equations of motion for K and ΔS, after rescaling, appear just as in Eqs. (2.12) and (2.13) but expressed in terms of the new dimensionless variables κ and Δs.

III. NEEDLE CRYSTALS

We now wish to find shape-preserving steady-state growth forms, the so-called "needle crystals," that move with constant growth velocity v_0 in the z direction as shown in Fig. 4.

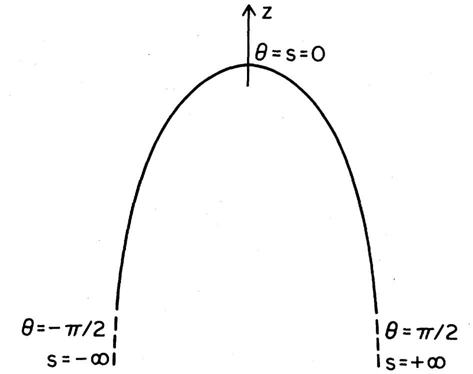

FIG. 4. Needle-crystal trajectory.

The motivation here, in looking for needle crystals, is that the dendrites obtained in the laboratory exhibit smooth tips at least for some finite portion of arclength, after which the side-branching activity becomes important. Needle crystals were first discovered by Ivantsov[12] in his study of the dendritic growth of a pure substance, for zero surface tension ($d_0=0$). He found a family of parabolic shapes where the tip velocity v_0 and the tip curvature κ_0 obey the relation

$$\frac{v_0}{\kappa_0} = C \tag{3.1}$$

and C is a constant uniquely determined by the thermal undercooling $(T_M - T_\infty)/(L/C_p)$. In a situation where impurities are present the Ivantsov result can be generalized[7] and a relation identical to Eq. (3.1) holds, except that C is now uniquely determined by Δ_e and βC_∞. These results are exact but only valid when $d_0=0$. However, we know that the surface tension plays a crucial role in the pattern formation of dendrites, since it restabilizes short-wavelength perturbations.

Recent studies of local models of interface dynamics[5,6] have given us a good clue to what happens when $d_0 \neq 0$. In particular, it was found that in this case only a discrete set of needle crystals could exist. Furthermore, the member of this discrete set with the maximum velocity corresponded to the state selected in numerical simulations of the dynamical models studied. Our aim here is to elucidate if needle crystals can be found when impurities are present. To do so we look for shape-preserving solutions of Eqs. (2.14)–(2.17) with $v_n = v_0\cos\theta$ and $\partial h_i/\partial\tau|_s = 0$ $(i=1,2)$ as shown in Fig. 4. The later constraints simply say that at steady state h_i remains invariant, at constant s, in a frame which moves at speed v_0. The relation between the constant s and normal time derivative for steady state is simply

$$\left.\frac{d}{d\tau}\right|_n = \left.\frac{\partial}{\partial\tau}\right|_s + v_0\sin\theta\,\partial_s\,. \tag{3.2}$$

Setting $v_n = v_0\cos\theta$, $\partial h_i/\partial\tau|_s = 0$, and eliminating $d/d\tau|_n$ in Eqs. (2.14) and (2.15) we obtain, after some simple algebraic manipulations, the steady-state equations describing shape-preserving growth forms. To describe the needle-crystal trajectories it is convenient to write down the steady-state equations as an autonomous system of five coupled ordinary-differential equations (ODE's) with dependent variables u_1, u_2, $\lambda_1 \equiv du_1/ds$, $\lambda_2 \equiv du_2/ds$, θ, and independent variable s:

$$\frac{d\theta}{ds}=\kappa=(\Delta_e-u_1-\beta C_\infty u_2)/(1+f)\ , \tag{3.3}$$

$$\frac{du_1}{ds}=\lambda_1\ , \tag{3.4}$$

$$\frac{du_2}{ds}=\lambda_2\ , \tag{3.5}$$

$$\frac{d\lambda_1}{ds}=\frac{\kappa u_1 v_0}{\cos\theta}-v_0^2\cos^2\theta\left[\frac{1-u_1}{u_1}\right] -\lambda_1(\kappa\tan\theta-2v_0\sin\theta)-\frac{\lambda_1^2}{u_1}\ , \tag{3.6}$$

$$\frac{d\lambda_2}{ds}=\frac{\kappa u_2 v_0}{r\cos\theta}-\frac{v_0^2\cos^2\theta}{r^2}\left[\frac{1+u_2}{u_2}\right] -\lambda_2\left[\kappa\tan\theta-\frac{v_0\sin\theta}{r}\left[\frac{2+u_2}{1+u_2}\right]\right] -\frac{\lambda_2^2}{u_2(1+u_2)}\ . \tag{3.7}$$

Note that v_0 enters here only as an external parameter.

We now discuss qualitatively the properties of the set of equations (3.3)–(3.7). In this way we hope to give some intuition for the problem of finding needle crystals and also give some motivation for the asymptotic analysis that will follow. First, consider the simpler problem of finding needle-crystal solutions in the case of a pure substance ($\beta C_\infty=0$). In this case only the variables θ, u_1, and λ_1 enter together with Eqs. (3.3), (3.4), and (3.6). There are two physical fixed points of this set of equations at $\theta=\pm\pi/2$, $u_1=\Delta$, and $\lambda_1=0$. Needle-crystal solutions correspond to trajectories that leave the $\theta=-\pi/2$ fixed point and intersect the $\theta=0$ plane at $\lambda_1=0$. Since the steady-state equations are invariant under reflection symmetry about the z axis ($\theta=0$), these trajectories will necessarily flow into the other fixed point at $\theta=\pi/2$. In what follows we will only refer to the $\theta=-\pi/2$ fixed point but everything that will be said also applies to the other fixed point. A detailed study of the $\theta=-\pi/2$ fixed point shows that only a single trajectory flows out of this fixed point for a given value of v_0.[4] In general, this trajectory will not intersect the $\theta=0$ plane at $\lambda_1=0$ unless v_0 has special values. Therefore, at best, only a discrete set of needle crystals can exist. We now turn to the situation where impurities are present ($\beta C_\infty\neq 0$). In this case the phase space is five-dimensional and needle-crystal solutions correspond to trajectories that leave the $\theta=-\pi/2$, $u_1=u_1^*$, $u_2=u_2^*$, $\lambda_1=\lambda_2=0$ fixed point and intersect the $\theta=0$ hyperplane at $\lambda_1=0$ and $\lambda_2=0$. (The fixed-point values u_1^* and u_2^* will be determined below.) Consequently, in general for needle crystals to exist we need at least two free parameters to satisfy the two conditions $\lambda_1=0$ and $\lambda_2=0$. The first free parameter is as before the tip velocity v_0. The second free parameter will be shown to exist below and follows from the finding that a single-parameter family of trajectories leave the $\theta=-\pi/2$ fixed point (when $\beta C_\infty\neq 0$).

The existence of two free parameters is only a necessary condition for the existence of needle crystals when $\beta C_\infty\neq 0$. One then needs to construct these solutions explicitly by direct numerical integration of Eqs. (3.3)–(3.7). That is, one needs to show that $\lambda_1=0$ and $\lambda_2=0$ can be satisfied simultaneously at the tip by adjusting v_0 and the free parameter at the fixed point. The details of this construction will be discussed later in this section.

We now wish to study the $\theta=-\pi/2$ fixed point when $\beta C_\infty\neq 0$ and demonstrate mathematically the existence of a single-parameter family of trajectories that flow out of this fixed point. For this purpose it is more convenient to eliminate the s coordinate in terms of a new coordinate $x\equiv\cos\theta$ which can serve as an expansion variable in the neighborhood of the fixed point, and rewrite the steady-state equations (3.3)–(3.7) as two coupled second-order ODE's in the new variable x. After simple algebraic manipulations we obtain

$$v_0^2x^2\left[\frac{u_1\kappa}{v_0x^3}-\frac{1-u_1}{u_1}\right]-\frac{\partial u_1}{\partial x}\left[2v_0\kappa(1-x^2)-\frac{\kappa^2}{x}+\kappa(1-x^2)\frac{\partial\kappa}{\partial x}+\kappa^2\frac{(1-x^2)}{u_1}\frac{\partial u_1}{\partial x}\right]-\kappa^2(1-x^2)\frac{\partial^2 u_1}{\partial x^2}=0\ , \tag{3.8}$$

$$\frac{v_0^2x^2}{r^2}\left[\frac{ru_2\kappa}{v_0x^3}-\frac{1+u_2}{u_2}\right]-\frac{\partial u_2}{\partial x}\left[\frac{v_0(1-x^2)\kappa(2+u_2)}{r(1+u_2)}-\frac{\kappa^2}{x}+\kappa(1-x^2)\frac{\partial\kappa}{\partial x}+\frac{\kappa^2(1-x^2)}{u_2(1+u_2)}\frac{\partial u_2}{\partial x}\right]-\kappa^2(1-x^2)\frac{\partial^2 u_2}{\partial x^2}=0\ , \tag{3.9}$$

$$[1+8\alpha x^2(1-x^2)]\kappa=\Delta_e-u_1-(\beta C_\infty)u_2\ . \tag{3.10}$$

Equations (3.8) and (3.9) are the heat and solute boundary-layer equations at steady state and Eq. (3.10) is the Gibbs-Thomson relation with a simple choice of a fourfold anisotropy ($m=4$).

A first step in the study of the $x=0$ fixed point is to extract the leading behavior of κ as a function of x and the fixed-point values of temperature and concentration u_1^* and u_2^*. To do so we note that the leading singularity in Eqs. (3.8) and (3.9) has to vanish as $x\rightarrow 0$ [first term in square brackets in Eqs. (3.8) and (3.9)]. Any other possibility leads to an inconsistency in which u_1 and u_2 diverge at $x=0$. This implies that $\kappa=\kappa^*x^3$ to leading order in x.

Setting the main singularities equal to zero [first term in large parentheses in Eqs. (3.8) and (3.9)] we have

$$\frac{\kappa^*}{v_0}=\frac{1-u_1^*}{(u_1^*)^2}\ , \tag{3.11}$$

$$\frac{r\kappa^*}{v_0}=\frac{1+u_2^*}{(u_2^*)^2} \; . \tag{3.12}$$

From the Gibbs-Thomson condition we also have

$$u_1^*+(\beta C_\infty)u_2^*=\Delta_e \; . \tag{3.13}$$

Equations (3.11)—(3.13) determine u_1^*, u_2^*, and κ^* uniquely. At zero surface tension $d_0=0$ the isothermal and isoconcentration trajectories $\kappa=\kappa^* x^3$, $u_1=u_1^*$, and $u_2=u_2^*$ are the exact Ivantsov parabolic trajectories for our model.

To investigate the properties of the fixed point further ($d_0\neq 0$) we write κ, u_1, and u_2 in a power-series expansion in x of the following form:

$$\kappa=x^3 \sum_{\substack{(n,n)\\ 0\leq n,m\leq\infty}} \kappa(n,m)x^{n+m\delta} \; , \tag{3.14}$$

$$u_i=\sum_{\substack{(n,m)\\ 0\leq n,m\leq\infty}} u_i(n,m)x^{n+m\delta} \quad (i=1,2) \; . \tag{3.15}$$

Here we have allowed for the possibility of noninteger powers of x. We shall see shortly that this inclusion turns out to be crucial here. Next we substitute Eqs. (3.14) and (3.15) into Eqs. (3.8)—(3.10), expand, and solve for the $\kappa(n,m)$ and $u_i(n,m)$. At lowest order we recover $\kappa(0,0)=\kappa^*$, $u_i(0,0)=u_i^*$ $(i=1,2)$. Now at the lowest order in the expansion where δ first appears we obtain $(\beta C_\infty\neq 0)$

$$\begin{bmatrix} \dfrac{v_0}{(u_1^*)^2}[(1-2\delta)(1-u_1^*)+1] & u_1^* \\ -\dfrac{v_0}{r(\beta C_\infty)(u_2^*)^2}[(1-\delta)(2+u_2^*)] & u_2^* \end{bmatrix} \begin{bmatrix} u_1(0,1) \\ \kappa(0,1) \end{bmatrix} = 0 \; , \tag{3.16}$$

where we have eliminated $u_2(0,1)$ in favor of $u_1(0,1)$ via the Gibbs-Thomson relation

$$u_1(0,1)+(\beta C_\infty)u_2(0,1)=0 \; . \tag{3.17}$$

Now the heart of our argument is that given Δ_e, βC_∞, and r, for a particular value of δ the determininant of the matrix A [defined by Eq. (3.16)] vanishes. Setting $\det A=0$ and solving for δ we obtain at once

$$\delta=1+\frac{r u_1^*(\beta C_\infty)(u_2^*)^3}{[2(1-u_1^*)r(\beta C_\infty)(u_2^*)^3+(2+u_2^*)(u_1^*)^3]} \; . \tag{3.18}$$

Since $\det A=0$, $u_1(0,1)$ is undetermined and consequently a one-parameter family of trajectories leave (or approach) the $x=0$ fixed point, tangent to the Ivantsov trajectory $\kappa=\kappa^* x^3$, $u_1=u_1^*$, $u_2=u_2^*$. Note that δ defined by Eq. (3.18) is always positive, which is consistent with the requirement that u_1 and u_2 remain finite at $x=0$. In the case where δ is an integer, which can occur for special values of βC_∞, Δ_e, and r, and for special values of this integer such that Eq. (3.17) involves the coefficient $\kappa(0,1)$ (for example, if $\delta=3$) the above analysis has to be generalized to include logarithms $(x^n \ln x)$ in the expansion. However, we still find a one-parameter family of trajectories and the details of this special case are shown in Appendix B. A plot of $\delta-1$ versus βC_∞ for $\Delta_e=0.2, 0.5, 0.8$ and $r=0.01$ is shown in Fig. 5.

The trajectories which leave the $x=0$ fixed point are characterized by surface temperature and concentration profiles u_1 and u_2 of the form

$$\begin{aligned} u_1 &= u_1^*+u_1(0,1)x^\delta+u_1'(x) \; , \\ u_2 &= u_2^*-\frac{u_1(0,1)}{(\beta C_\infty)}x^\delta+u_2'(x) \; , \end{aligned} \tag{3.19}$$

where

$$u_i'(x)=\sum_{\substack{(n,m)\ [\neq(0,0),(0,1)]\\ 0\leq n,m\leq\infty}} u_i(n,m)x^{n+m\delta} \tag{3.20}$$

is determined uniquely in terms of $u_1(0,1)$ (which is arbitrary) and Δ_e, βC_∞, and r. To see this, when we eliminate $u_2(n,m)$ in favor of $u_1(n,m)$ via Eq. (3.10) we find, at each order in the expansion, the following structure:

$$\begin{bmatrix} b_{11} & b_{12} \\ b_{22} & b_{22} \end{bmatrix} \begin{bmatrix} u_1(n,m) \\ \kappa(n,m) \end{bmatrix} = \begin{bmatrix} c_1 \\ c_2 \end{bmatrix} \; , \qquad (n,m)\neq(0,0);(0,1) \tag{3.21}$$

with $\det B\neq 0$ and the b_{ij}'s and c_i's uniquely determined in terms of previous coefficients $u_1(n',m'),\kappa(n',m')$ where $n'+m'\delta<n+m\delta$. Since now δ is fixed [Eq. (3.18)], in general $\det B\neq 0$ and the $u_1(n,m)$ and $\kappa(n,m)$ are all uniquely determined. We verified that $\det B\neq 0$ for the next few orders in the fixed-point expansion. Also we integrated the system of ODE's Eqs. (3.3)—(3.7) near the fixed point $(x=0.01)$ and measuring the slope of $\ln|\partial u_i/\partial x|$ plotted versus $\ln x$ (slope $=\delta-1$) we found δ to agree with Eq. (3.18) within less than 1% for different values of $u_1(0,1)$, Δ_e, βC_∞, and r.

We now would like to discuss the physical meaning of the free parameter $u_1(0,1)$, the explicit construction of needle-crystal solutions, and the limit of zero impurity concentration $(\beta C_\infty \rightarrow 0)$.

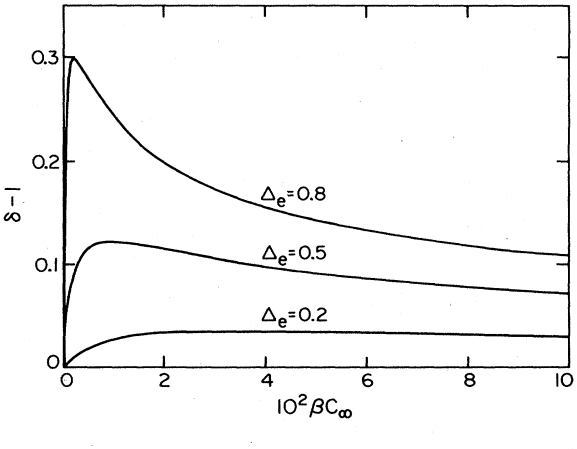

FIG. 5. $\delta-1$ vs βC_∞ for $\Delta_e=0.2$, 0.5, and 0.8. $r=0.01$.

The physical meaning of $u_1(0,1)$ is contained in the Gibbs-Thomson relation, Eq. (3.10). When $\beta C_\infty \neq 0$ the surface temperature u_1 and concentration u_2 can be adjusted without affecting the surface tension, namely the curvature, simply by sliding along the liquidus. This statement is contained in Eq. (3.17). At $\beta C_\infty = 0$ the temperature cannot be adjusted independently of the curvature and in this more stringent situation only a single trajectory leaves the fixed point.

To construct the needle-crystal solutions for given values of Δ_e, βC_∞, and r we proceed as follows. We first fix v_0 and find the value of $u_1(0,1)$ such that $\lambda_2(\theta=0)=0$. This is done by integrating numerically the system of ODE's (3.3)–(3.7) from the fixed point to the tip. In practice, we start close to the fixed point $(x=0.1)$ and move our starting point closer to the fixed point until the values at the tip have converged sufficiently. For a given v_0 the value of $\lambda_1(\theta=0) \equiv \tilde{\lambda}_1(v_0)$ such that $\lambda_2(\theta=0)=0$ is, in general, nonzero. We then repeat this procedure for different values of v_0 and plot $\tilde{\lambda}_1(v_0)$ versus v_0. The zero crossings of this curve correspond to the needle crystals. The crossing with the maximum velocity determines the special velocity $v_0 = v_0^*$ and its corresponding tip curvature $\kappa_0(\theta=0)=\kappa_0^*$. A plot of $\tilde{\lambda}_1(v_0)$ versus v_0 in the neighborhood of v_0^* for $\Delta_e = 0.9$, $\beta C_\infty = 0.01$, $r=0.2$, and $\alpha = 0.1$ is shown in Fig. 6.

We now discuss the limit of zero solute concentration $\beta C_\infty \to 0$. In the case of a pure substance $u_1(0,1)=0$, and a single trajectory leaves the fixed point. When $\beta C_\infty \neq 0$, no matter how small, $u_1(0,1)$ is arbitrary and a one-parameter family of trajectories leave the fixed point. In this sense the nature of the fixed points $(\theta = \pm\pi/2)$ changes discontinuously as impurities are added. This feature can be regarded as a mathematical property of the fixed points. However, the important physical limit here, which relates to the shape and velocity of the needle-crystal solutions as $\beta C_\infty \to 0$, is continuous. This follows from a simple scaling observation. For any value of x, no matter how small, $u_2(x)$ has to remain finite as $\beta C_\infty \to 0$. Since $\delta \to 1$ as $\beta C_\infty \to 0$ it follows from Eq. (3.19) that the only possibility is that $u_1(0,1)$ vanishes at least as fast as βC_∞ for $u_2(x)$ to remain finite. Consequently, the needle-crystal solutions at various βC_∞ for fixed Δ_e and r approach the pure thermal needle crystal smoothly as $\beta C_\infty \to 0$. We verified this conjecture numerically and found that $u_1(0,1)$ had to be made increasingly smaller to construct a needle crystal as $\beta C_\infty \to 0$.

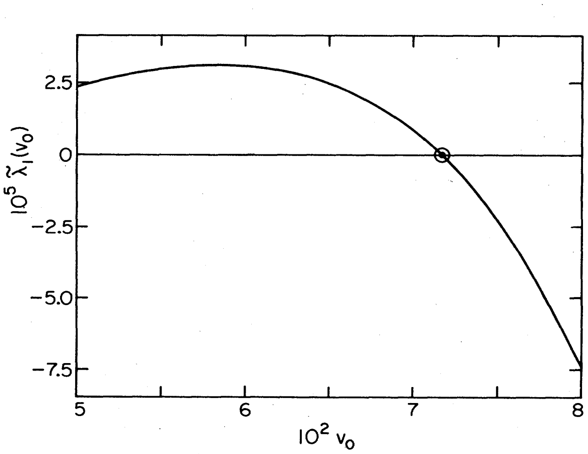

FIG. 6. $\tilde{\lambda}_1(v_0)$ vs v_0 for $\Delta_e = 0.9$, $\beta C_\infty = 0.01$, and $r=0.2$. The zero crossing identifies the needle-crystal solution and the selected velocity v_0^*.

Finally, we mention that since δ is, in most cases, noninteger and slightly greater than 1, one could object that $\partial^2 u_i/\partial x^2$ diverges at $x=0$. This singularity is of no physical consequence whatsoever since all physical derivatives involve the gradient along the interface ∂_s, and $\partial_s \simeq x^3(\partial/\partial x)$ $(x \ll 1)$. Consequently, $\partial_s^n u_i$ is always finite for all n.

IV. NUMERICAL SIMULATION

To investigate the relevance of the needle-crystal solutions to the dynamics of our model we integrate numerically the system of equations (2.12)–(2.17) by using an algorithm very close to the one that was developed in Ref. 4. The difference here is that we also have to track an extra field, namely the solute concentration. The essence of the algorithm is that instead of using a two-dimensional grid in real space it is easier to track the interface using curvature as a function of arclength $\kappa(s,t)$. This reduces the dimensionality of the numerical problem by 1. The new difficulty that arises, however, is that the arclength is tim dependent. This problem is shown in Fig. 7, where we have shown a portion of interface at two different times Δt apart.

In places of positive (negative) curvature the local grid spacing Δs_i stretches (shrinks). To avoid this difficulty the grid points are redistributed equally along the arclength at each time step and the values of the fields $\kappa, h_1, h_2, \ldots$ are interpolated to identify their values at the new, equally spaced points. Another problem that arises is that the fields u_1 and u_2 cannot be easily eliminated in terms of h_1 and h_2. If one attempts this elimination by combining Eqs. (2.16) and (2.17), one is left with a quartic equation with no simple roots. To circumvent this problem u_2 is eliminated in terms of u_1, h_1, and h_2 by solving a simple quadratic equation, and u_1 is treated artifically as a dynamical field in the implicit scheme by Taylor-series expanding the Gibbs-Thomson relation Eq. (2.17). The algorithm can be summarized as follows. First, the five fields κ, Δs, h_1, h_2, and u_1 are time-stepped forward using an implicit scheme:

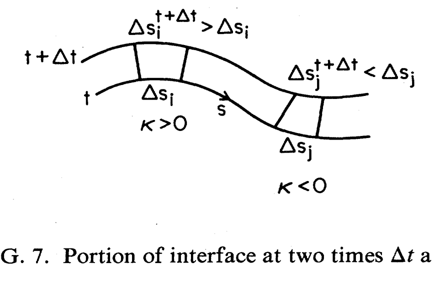

FIG. 7. Portion of interface at two times Δt apart.

$$\frac{\psi^{t+\Delta t}-\psi^{t}}{\Delta t}=\tfrac{1}{2}F[\psi]\,|_{t}+\tfrac{1}{2}F[\psi]\,|_{t+\Delta t}\,, \qquad (4.1)$$

where ψ is the $5N$-dimensional vector (i.e., 5 fields and N grid points) and F is the nonlinear operator defined by the equations of motion (2.12)–(2.17). Equation (4.1) is Taylor-series expanded about t and the resulting set of coupled linear equations are solved by upper-diagonalization. Then Δs is redistributed equally along the arclength and the four fields κ, h_1, h_2, and u_1 are interpolated by a simple cubic-spline routine. Step 1 is then restarted.

Another problem we have to overcome in doing our numerical simulations is that the boundary-layer model, as it stands, cannot describe the physics of the grooves that form on the sides of the dendrite. Numerically this deficiency of the model translates into a strong numerical instability when the groove becomes too deep. In this present paper, however, we are only interested in the tip properties, and this problem can be circumvented by keeping only a finite portion of arclength behind the tip, up to where the grooves become too deep. In this way, a tip steady state can be reached without the algorithm failing. To convince ourselves that the steady-state tip reached using this procedure was insensitive to the position behind the tip of the truncation of the interface, we repeated the simulations with different arclengths behind the tip and found that the steady state was not altered. This indicates that the steady-state tip is rather insensitive to perturbations down the side of the dendrite. Although this procedure seems adequate to describe the tip properties it cannot be used to describe the repeated formation of side branches, if present in the model. In order to remove this deficiency, there is presently work in progress trying to modify the boundary-layer model.

Using the procedures outlined above, we performed a very careful numerical experiment at $\Delta_e=0.9$, $\beta C_\infty=0.01$, and $r=0.2$. We also used a value of anisotropy sufficient to attain a steady state: $\alpha=0.1$. We found that the state selected dynamically shared the same tip properties as the needle crystal with the maximum velocity. That is, we found $v_{\text{expt}}=v_0^*$ and $\kappa_{\text{expt}}=\kappa_0^*$ (with a discrepancy less than 1%), where v_{expt} and κ_{expt} are, respectively, the values of tip velocity and tip curvature found in the numerical experiment, and $v_0^*=7.18\times10^{-2}$ and $\kappa_0^*=3.35\times10^{-2}$ are, respectively, the tip velocity and tip curvature of the corresponding needle-crystal solutions (see Fig. 6). This is in complete agreement with the previous results obtained for the geometrical model and the single-field boundary-layer model.[5,6]

V. DISCUSSION AND CONCLUSIONS

In the preceding sections we have studied a boundary-layer model to show that a solvability condition can be used to predict exactly the tip velocity v_0^* and the tip curvature κ_0^*, selected dynamically in the impurity problem. To explore the properties of our model further and make contact, at least qualitatively, with real solidification experiments, we have studied the dependence of v_0^* and κ_0^* on solute concentration. For this purpose we have chosen $\Delta_e=0.5$, $r=0.01$ (typically for a liquid mixture $r\sim10^{-2},10^{-3}$), and a strength of anisotropy sufficient to insure a steady state $\alpha=0.1$. To check that this strength of anisotropy was sufficient to reach a steady state we performed a numerical simulation, as described in Sec. IV, for $\Delta_e=0.5$, $r=0.01$, $\beta C_\infty=0.002$, and found that a constant tip velocity and tip curvature were reached in quantitative agreement with the predictions from the solvability condition. We have then calculated v_0^* and κ_0^* as functions of impurity concentration βC_∞ using the solvability condition and the needle-crystal construction discussed in Sec. III. Our results are shown in Fig. 8. We find at small impurity concentration a sharp enhancement in tip velocity in good qualitative agreement with real solidification experiments.[10] We emphasize that, in the context of the boundary-layer model, which is valid in the limit of large undercoolings and in two dimensions, we cannot hope to predict quantitatively the results of experiments which are done at small undercoolings and in three dimensions. However, this good qualitative agreement in the tip-velocity enhancement is very suggestive of the relevance of our model and its mathematical properties to the more complex three-dimensional and highly nonlocal situations. The physics of this velocity enhancement can be understood in terms of a competition between two effects. On one hand, as impurities are added, a thin boundary layer of impurities is formed around the tip. This solute boundary layer is thinner by a factor of r than the thermal boundary layer and will tend to sharpen the tip, thereby enhancing the growth velocity. This tip sharpening is displayed in Fig. 8(b), also in good qualitative agreement with experiments. On the other hand, impurities diffuse much slower than heat by a factor of r, and this second effect will tend to retard the growth velocity. The relative strength of these two competing effects determine the magnitude of the velocity enhancement.

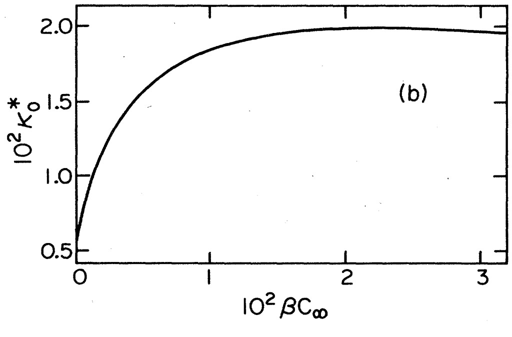

FIG. 8. (a) v_0^* and (b) κ_0^* vs βC_∞ for $\Delta_e=0.5$, $r=0.01$, and $\alpha=0.1$.

Previous theories of the impurity effect[7–9] captured the essence of this competition by selecting, out of a family of parabolic growth forms, the state with a marginally stable tip. They were thereby successful in giving us a crude estimate of the velocity enhancement. However, from a fundamental point of view it is clear, at least in the context of our model, that the operating point is not selected from a family of parabolic shapes but needs to be identified via a solvability condition. It still remains to be shown if this solvability condition generalizes to the full nonlocal free-boundary problem, but our qualitative agreement with experiment shown in Fig. 8 supports the validity of this conjecture.

In this paper we have concentrated on the properties of the tip. Questions related to the strong variations in sidebranching activity with solute concentration, seen experimentally,[10] still remain to be studied.

We have also used here a strength of anisotropy, α, sufficient to insure a steady-state tip in the numerical simulation. It has been shown in the context of the geometrical model that when $\alpha < \alpha_c$ the needle-crystal solutions become unstable. A similar threshold is likely to exist in our model and it would be feasible to study the dependence of α_c on solute concentration by performing a detailed stability analysis of the needle-crystal solutions.

In conclusion, we have studied a boundary-layer model of dendritic growth in the presence of impurities, and we have shown that the solvability criterion propose recently for the dendritic growth of a pure substance generalizes to this more complex situation. This is revealed mathematically by the existence of a one-parameter family of trajectories which flow in or out of the fixed points of the steady-state equations. Furthermore, our model predicts a tip-velocity enhancement at small impurity concentration which has been observed experimentally. This qualitative agreement is consistent with the conjecture that the new velocity selection criterion applies to the full nonlocal free-boundary problem.

ACKNOWLEDGMENTS

We are grateful to E. Ben-Jacob, N. Goldenfeld, Professor J. S. Langer, M. Marder, and P. Voorhees for helpful discussions. We also would like to thank E. Ben-Jacob and N. Goldenfeld for providing part of the program code that was used in our numerical simulations. This material is based upon research supported by the U.S. Department of Energy under Grant No. DE-FG03-84ER45108 and the National Science Foundation under Grant No. PHY-77-27084, supplemented by funds from the U.S. National Aeronautics and Space Administration.

APPENDIX A

Consider a plane growing in the η direction with instantaneous velocity v_n. In this case we have

$$\frac{dH_i}{dt} = -\dot{\eta}_0 u_i + \int_{\eta_0}^{\infty} \frac{\partial \tilde{u}_i(\eta,t)}{\partial t} d\eta = -V_n u_i + D_i \int_{\eta_0}^{\infty} \frac{\partial^2 \tilde{u}_i(\eta,t)}{\partial \eta^2} d\eta \; . \tag{A1}$$

Integrating by parts and eliminating the normal gradient $\partial \tilde{u}_i / \partial \eta$ at the interface via the continuity equations (2.5) and (2.6) we obtain at once

$$\frac{dH_i}{dt} = V_n(1 - u_i \delta_{1,i}) \; . \tag{A2}$$

APPENDIX B

In the special case where δ defined by Eq. (3.18) is an integer which coincides with a nonvanishing power of κ, our analysis has to be modified slightly. The important feature of a single-parameter family of trajectories remains unchanged, however. To understand the problem consider the simple first-order linear ODE:

$$\frac{\partial \psi}{\partial x} - \delta \frac{\psi}{x} = x^2 \; . \tag{B1}$$

It has a simple solution when $\delta \neq 3$:

$$\psi = \psi^0 x^\delta + \frac{x^3}{3-\delta} \; , \tag{B2}$$

where ψ^0 is arbitrary. When $\delta = 3$ a simple power-series method breaks down, and we have

$$\psi = \psi^0 x^3 + x^3 \ln x \; . \tag{B3}$$

The same problem occurs in our fixed point analysis of Sec. III. Consider, for example, the case where $\delta = 3$. In this case, the right-hand side of Eq. (3.16) is nonzero since $u_2(0,1)$ depends on both $u_1(0,1)$ and κ^*. Yet the determinant of the matrix A on the left-hand side of (3.16) vanishes and we are left with no solutions for $u_1(0,1)$ and $\kappa(0,1)$. To remove this difficulty we assume an expansion of the form

$$\begin{aligned} u_i(x) &= u_i^* + u_i(3)x^3 + u_i'(3)x^3 \ln x + \cdots \; , \\ \kappa(x) &= \kappa^* x^3 + \kappa_6 x^6 + \kappa_6' x^6 \ln x + \cdots \; . \end{aligned} \tag{B4}$$

Substituting (B4) into Eqs. (3.8)—(3.10), we obtain a system of two coupled homogeneous and nonhomogeneous equations with vanishing determinant relating the undermined coefficients:

$$\begin{bmatrix} a_{11} & a_{12} \\ a_{21} & a_{22} \end{bmatrix} \begin{bmatrix} u_1'(3) \\ \kappa_6' \end{bmatrix} = 0 \tag{B5}$$

and

$$\begin{bmatrix} a_{11} & a_{12} \\ a_{21} & a_{22} \end{bmatrix} \begin{bmatrix} u_1(3) \\ \kappa_6 \end{bmatrix} = \begin{bmatrix} a u_1'(3) \\ -b u_1'(3) + c \end{bmatrix} \tag{B6}$$

with $\det \underline{A} = 0$ and a, b, and c uniquely determined in terms of $u_i^*, \kappa^*, \ldots$. From Eq. (B5) $u_1'(3)$ is arbitrary. For Eq. (B6) to have a solution we need

$$u_1'(3) = \frac{c}{b + (a_{22}/a_{12})a} \; . \tag{B7}$$

Then $u_1(3)$ is arbitrary (one-parameter family) and $u_1'(3)$ is determined.

[1] J. S. Langer, Rev. Mod. Phys. **52**, 1 (1980).

[2] R. Brower, D. Kessler, J. Koplik, and H. Levine, Phys. Rev. Lett. **51**, 1111 (1983); Phys. Rev. A **29**, 1335 (1984).

[3] H. Müller-Krumbhaar, in Proceedings of the NATO Workshop on Chemical Instabilities, Austin, Texas, 1983 (in press).

[4] E. Ben-Jacob, N. Goldenfeld, J. S. Langer, and G. Schön, Phys. Rev. Lett. **51**, 1930 (1983); Phys. Rev. A **29**, 330 (1984).

[5] D. Kessler, J. Koplik and H. Levine, Phys. Rev. A **31**, 1712 (1985).

[6] E. Ben-Jacob, N. Goldenfeld, B. G. Kotliar, and J. S. Langer, Phys. Rev. Lett. **53**, 2110 (1984).

[7] J. S. Langer, Physiochem. Hydrodyn. **1**, 41 (1980).

[8] A. Karma and J. S. Langer, Phys. Rev. A **30**, 3147 (1984).

[9] J. Lipton, M. E. Glicksman, and W. Kurz, Mater. Sci. Eng. **65**, 37 (1984).

[10] M. A. Chopra, Ph.D. thesis, Rensselaer Polytechnic Institute, 1983.

[11] J. S. Langer and L. A. Turski, Acta Metall. **25**, 1113 (1977).

[12] G. D. Ivantsov, Dokl. Akad. Nauk SSSR **58**, 567 (1947).